Rivista Italiana di Paleontologia e Stratigrafia
(*Research in Paleontology and Stratigraphy*)
vol. 130(3): 633-649. **November 2024**
DOI: https://doi.org/10.54103/2039-4942/22315

THE DEMISE OF THE MESSINIAN SALINITY CRISIS AND THE BEGINNING OF THE ZANCLEAN IN THE NORTHERN MEDITERRANEAN BASIN: INSIGHT FROM HIGH-RESOLUTION BIOMAGNETOSTRATIGRAPHY (POLLENZO SECTION, NW ITALY)

FRANCESCO PILADE*, FRANCESCA LOZAR, FRANCESCO DELA PIERRE, ELENA ZANELLA, ALAN MARIA MANCINI, MARCELLO NATALICCHIO, MATTEO MARCHISIO & ROCCO GENNARI

Dipartimento di Scienze della Terra, Università di Torino. Via Valperga Caluso 35, 10125 Torino (Italy)
*Corresponding Author: francesco.pilade@unito.it; ORCID-ID: https://orcid.org/0000-0003-1625-9570

Associate Editor: Giovanni Muttoni.

To cite this article: Pilade F., Lozar F., Dela Pierre F., Zanella E., Mancini A.M., Natalicchio M., Marchisio M. & Gennari R. (2024) - The demise of the Messinian salinity crisis and the beginning of the Zanclean in the northern Mediterranean basin: insight from high-resolution biomagnetostratigraphy (Pollenzo section, NW Italy). *Riv. It. Paleontol. Strat.*, 130(3): 633-649.

Keywords: Calcareous nannoplankton; Planktic foraminifera; cluster analysis; multivariate analysis; Milankovitch cycles; paleoenvironmental reconstruction.

Abstract: The Messinian-Zanclean boundary in the Mediterranean basin marks the end of the Messinian salinity crisis (MSC) at approximately 5.33 Ma. The mechanism behind the return to normal marine conditions after the MSC are debated, with two main hypotheses proposed: an instantaneous reflooding of the Mediterranean at the base of the Zanclean, following its near-complete desiccation, or a gradual sea level rise in a non-desiccated basin during the late MSC phase (Lago-Mare). Our objectives are to refine the age model of the Pollenzo section in the Piedmont basin, Italy, and to elucidate environmental variability during this phase. We employ high-resolution biomagnetostratigraphic and cyclostratigraphic analyses, integrated with statistical multivariate and cluster analyses, and tie the results with other Italian Mediterranean reference sections of the basal Zanclean. The proposed age model is based on biostratigraphic markers (planktic foraminifera and calcareous nannofossils), alongside the identification of the base of the Thvera subchron. Although no astrochronological tuning was proposed, the influence of orbital parameters variation on calcareous plankton was noted, especially at tie of eccentricity maxima. Our results indicate a gradual restoration of open marine conditions after the MSC, spanning from 5.33 to 5.23 Ma. We observe a transition from a more marginal environment to more open marine conditions at the termination of MSC.

Our findings challenge the notion of an abrupt transition at the end of the MSC, emphasizing the gradual nature of environmental change in the northernmost Mediterranean basin, from the late Messinian to the early Zanclean.

Received: January 16, 2024; accepted: September 17, 2024

Introduction

The transition from the Messinian to the Zanclean in the Mediterranean basin marks the demise of the Messinian salinity crisis (MSC; 5.97-5.33 Ma; CIESM, 2008; Roveri et al. 2014), during which the youngest salt giant of Earth history formed. The Messinian-Zanclean boundary (MZB) is marked by a sharp change in depositional facies from brackish sediments during the final stage of the crisis (Lago Mare event; 5.55-5.33 Ma; Roveri et al. 2014; Andreetto et al. 2021) to open marine sediments at the base of the Zanclean stage. The extensive research during the last fifty years led to the formulation of three hypotheses to explain the termination of the MSC and the alleged prominent lithological and paleontological shift: (a) the rapid (instantaneous) flooding at the beginning of the Zanclean of an almost desiccated Mediterranean basin, following the reopening of the connection with the Atlantic Ocean through the paleo-Gibraltar gateway (Hsü 1973; Blanc-Valleron et al. 2002; Garcia-Castellanos et al. 2009; García-Alix et al. 2016; Caruso et al. 2020; Amarathunga et al. 2022; Van Dijk et al. 2023; Ryan 2023); (b) the restoration of marine conditions in a non-desiccated Mediterranean after a gradual sea level rise during the latest MSC phase (Lago-Mare), which culminated in the complete restoration of the Atlantic-Mediterranean connection (Loget et al. 2005; Pierre et al. 2006; Roveri & Manzi 2006; Marzocchi et al. 2016; Carnevale et al. 2018; Andreetto et al. 2022; Carnevale & Schwarzhans 2022; Bulian et al. 2022b; Mancini et al. 2023; Pilade et al. 2023); c) a two-step flooding event starting with a glacioeustatic sea-level rise at 5.52 Ma, followed by a global sea-level drop at 5.4 Ma, and a subsequent rise, which led to the refilling of the Mediterranean in the earliest Pliocene (Pérez-Asensio et al. 2013).

Scenarios a and b align with the reestablishment of normal marine conditions at the base of the Zanclean, following the MSC; while scenario c suggests that marine conditions were already repeatedly established before the Zanclean (Pérez-Asensio et al. 2013). The return to a fully marine basin connected with the Atlantic Oceans was astrochronologically dated at 5.33 Ma in the Eraclea Minoa section, where the Zanclean GSSP was defined (Van Couvering et al. 2000). In detail, the GSSP definition globally corresponds to insolation cycle 510, five precessional cycles below the base of the normal magnetostratigraphic subchron Thvera (5.235 Ma; Gradstein et al. 2020).

Extensive biostratigraphic, magnetostratigraphic, and cyclostratigraphic studies were conducted in the Mediterranean basin on basal Zanclean sediments from both inland sections (Iaccarino et al. 1999; Pierre et al. 2006; Gennari et al. 2008; Riforgiato et al. 2008; Roveri et al. 2014; Lancis et al. 2015; Cornée et al. 2016; Caruso et al. 2020) and boreholes (Hilgen 1991; Lourens et al. 1996; Di Stefano et al. 1996, 2010). However, a detailed record of the Messinian-Zanclean transition is still lacking in the northernmost part of the Mediterranean.

The Pollenzo section is located in the Piedmont basin, which during the late Messinian represented the northernmost portion of the Mediterranean basin (Popov et al. 2004; Andreetto et al. 2022b). Here, the sedimentary succession records all the events of the MSC and the Messinian-Zanclean transition (e.g., Dela Pierre et al. 2011, 2016). Previous studies provided detailed information on this critical time interval from both outcrop sections (such as the Moncucco quarry; Trenkwalder et al. 2008; Violanti et al. 2011) and core samples (e.g., the Narzole borehole; Sturani 1978; Violanti et al. 2009), suggesting the presence of a hiatus in the uppermost Messinian sediments (Trenkwalder et al. 2008). However, a high-resolution age model of the basal Zanclean sediments, which is required to effectively correlate the northern sector of the Mediterranean with the rest of the basin, is not available yet.

In this study, we aim to improve our understanding of the lower Zanclean stage in the northernmost Mediterranean basin. To achieve this goal, we integrated magnetostratigraphic analysis with calcareous plankton micropaleontology of the sediments from the Pollenzo section, applying a multivariate statistical approach. Our objectives are to refine the age model and to detail the environmental variability of the Zanclean sediments of the northernmost part of the Mediterranean, during this critical time interval. We compared our results with those from other Mediterranean reference sections, including the Eraclea Minoa GSSP (Van Couvering et al. 2000), and the northern Apennine (Gennari et al. 2008). We particularly focused on the evolution of the calcareous plankton assemblages during the early phase of the Zanclean marine restoration and the related paleoceanographic and pa-

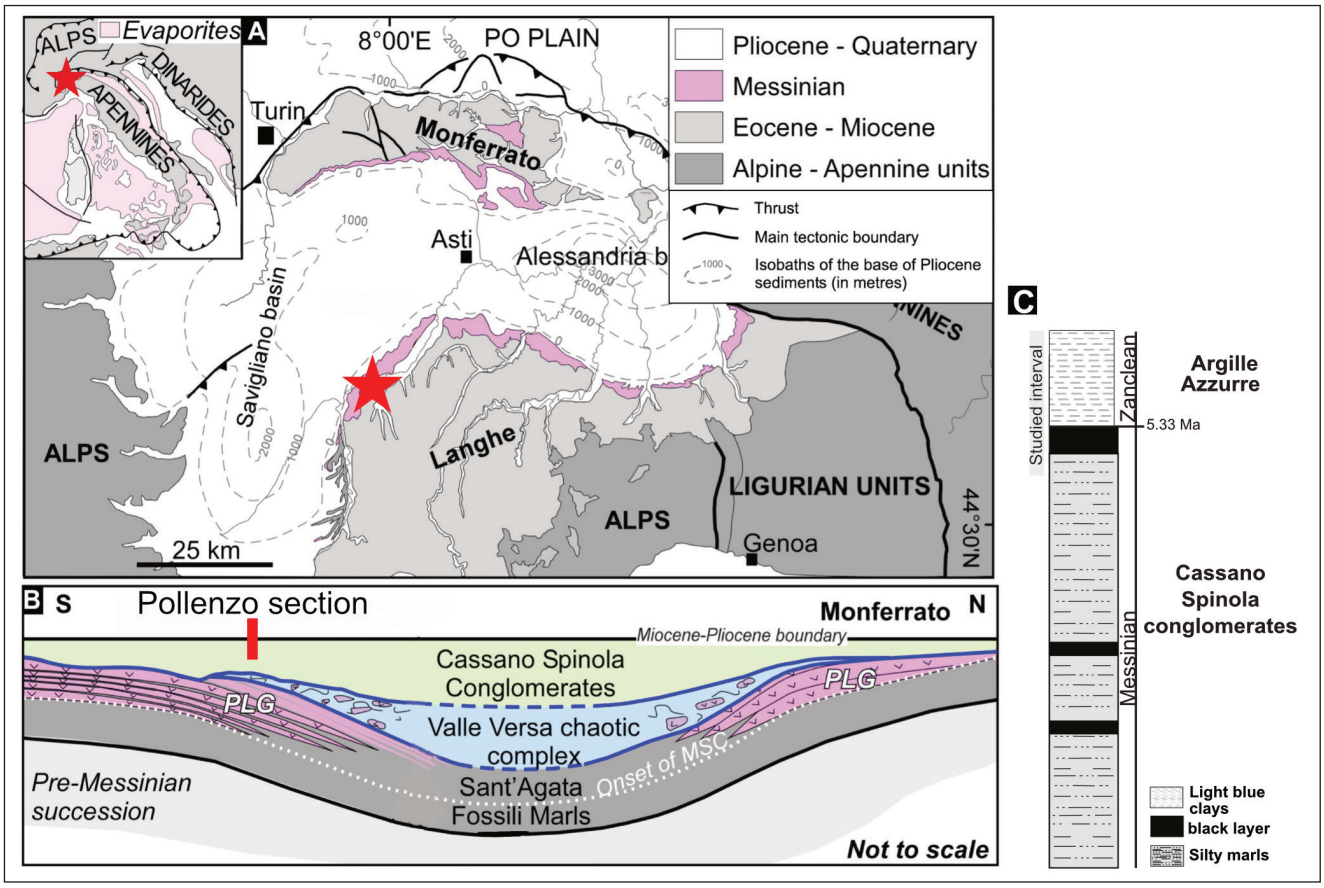

Fig. 1 - A) Simplified geological map of northwestern Italy (adapted from Sabino et al. 2020). The red star indicates the location of the Pollenzo section; B) schematic cross-section of the Piedmont basin, flattened at the base of the Pliocene, showing the relationships between the Messinian units (modified from Dela Pierre et al. 2011); PLG: Primary Lower Gypsum unit; C) simplified stratigraphic log of the upper Messinian and lower Zanclean deposits in the Pollenzo section (modified from Andreetto et al. 2022).

leoenvironmental changes. Ultimately, our research contributes to unravel the enigmatic termination of the MSC in the often-overlooked northern Mediterranean basin.

Geological setting

The Piedmont Basin (PB, Northwestern Italy) is a wedge-top basin situated on the inner side of the western Alpine chain (Fig. 1A). It is filled with a thick upper Eocene to Pliocene succession, deposited above a complex tectonic wedge formed by Alpine, Ligurian, and Adria basement units juxtaposed during the meso-alpine collisional event (Rossi et al. 2009; Mosca et al. 2010; Ghielmi et al. 2019).

In the Pollenzo section, the Messinian succession starts with the hemipelagic pre-MSC deposits of the Sant'Agata Fossili Marls (SAF; Lozar et al. 2010; Dela Pierre et al. 2011, 2012), which also include the onset of the MSC. Upward, the primary evaporitic deposits of the first stage of the MSC, referred to as the Primary Lower Gypsum unit, are capped by clastic evaporite deposits of the Valle Versa Chaotic Complex (Dela Pierre et al. 2011; Fig. 1B).

Primary and clastic evaporites are overlain by uppermost Messinian fluvio-deltaic to lacustrine terrigenous deposits that are referred to as the Cassano Spinola Conglomerates (CSC; see Andreetto et al. 2021, and references therein; Fig. 1b). The lower portion of the CSC consists of continental deposits with remains of terrestrial vertebrates (Colombero et al. 2017); the upper portion of the CSC (Fig. 1C) consists of silty marls with Lago-Mare fossil assemblages including gastropods such as *Melanopsis, Melanoides* and *Cerithium* and a mixture of brackish water ostracods of Paratethyan affinity, calcareous nannofossils and scattered foraminifera (Trenkwalder et al. 2008; Violanti et al. 2009, 2011; Andreetto et al. 2022). According to Andreetto et al. (2022), the calcareous nannofossil record just below the MZB

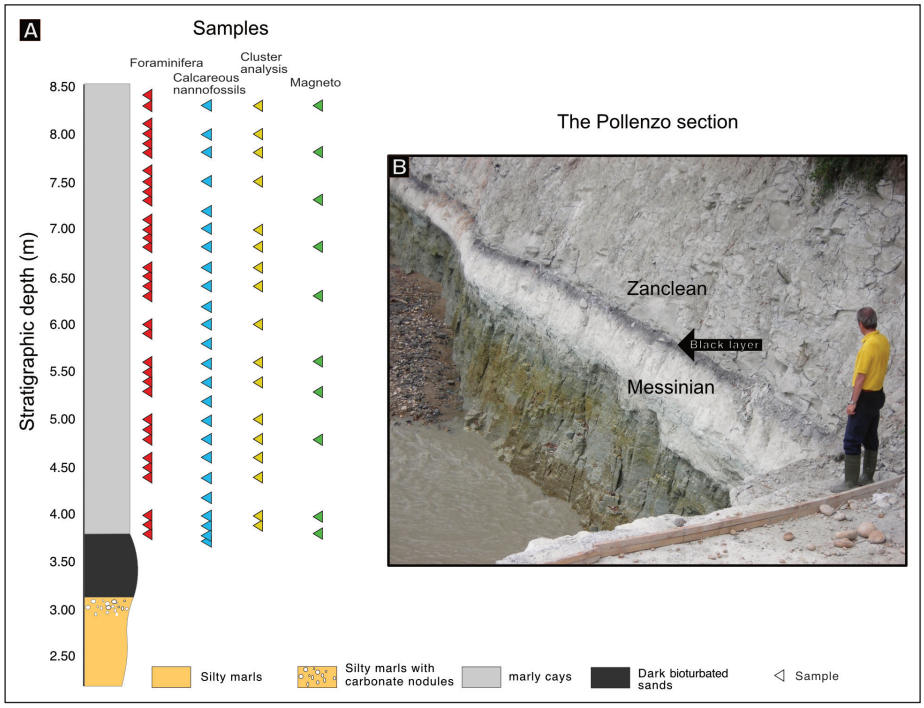

Fig. 2 - A) The studied Pollenzo section. Note the black layer separating the Messinian and Zanclean deposits. The arrows indicate the position of the samples; red: foraminifera; blue: calcareous nannofossils; yellow: micropaleontological samples chosen for cluster analysis; green: magnetostratigraphy; B) outcrop view of the studied section.

includes intact coccosphere which, although relatively uncommon, suggest that these marine fossils are autochthonous and not reworked. This evidence agrees with the gradual transgression suggested by Pilade et al. (2023) in the Northern Mediterranean and the capacity of coccolithophores to inhabit brackish waterbody connected to the sea (e.g. the Black Sea; Giunta et al. 2007). The transition to the Zanclean marly clays of the Argille Azzurre Formation (AAF) is marked by a highly bioturbated, glaucony and phosphate-rich black sandy layer. The AAF was deposited along the Northern Apennine margin and are rich in foraminifers and calcareous nannofossils generally indicating bathyal sedimentation depth (Carloni et al. 1974; Iaccarino & Papani 1979, and other; Colalongo 1988; Rio et al. 1990).

Material and methods

The Pollenzo section

The Pollenzo section (Figs. 1C and 2; 44°41'09.6" N, 7°54'50.4" E) is located on the left bank of the Tanaro River close to Verduno (CN). Nowadays the outcrop is submerged due to the recent construction of a dam. The thickness of the studied section is 8.6 m. The stratigraphic succession from bottom to top consists of: (a) 3.2 m of brown silty marls alternating with cm-thick layers of yellow sands (CSC); (b) 50 cm of silty marls characterized by the presence of carbonate nodules ranging in size from 1 mm to 20 cm (topmost part of CSC); (c) a black sandy layer of variable thickness (from 20 to 50 cm), marking the Messinian-Zanclean transition (Fig. S0); (d) 4.9 m of marly clays belonging to the AAF. Samples were collected during two surveys; planktic foraminifer (PF) and calcareous nannofossil (CN) samples differ in number and, in some cases, also differ in their stratigraphic position (see Fig. 2A).

Micropaleontological analyses

A total of 33 samples were collected for foraminifera, and a total of 24 samples were collected for calcareous nannofossils (Fig. 2A). In the case of foraminifera analysis, the samples were soaked in a solution of H_2O: H_2O_2 (9:1, in volume). The resulting residues were wet sieved to eliminate the clayey and silty fraction (< 63 μm) and were subsequently dry sieved to obtain three size fractions (>500 μm, 500-125 μm, and 125-63 μm).

Quantitative analyses of planktic foraminifer assemblages were carried out on the residues >125 μm. Residues were subdivided into aliquots by a splitter to obtain at least 300 specimens per sample and then handpicked. Taxonomic assignments were performed following the classifications of Schiebel and Hemleben (2017), Spezzaferri et al. (2018), Srinivasan & Kennett (1983), and Aze et al. (2011). Several species were grouped together: *Glo-*

boturborotalita group includes *G. apertura* Cushman, 1918, *G. decoraperta* (Takayanagi & Saito, 1962), *G. nepenthes* (Todd, 1957) and G. *woodi* Jenkins, 1960; the *Globigerinella* group includes both *G. obesa* (Bolli, 1957). and *G. pseudobesa* (Salvatorini, 1967); the *Globigerinita* group includes both *G. glutinata* Egger, 1893 and *G. uvula* (Ehrenberg, 1861); the *Globigerina* group includes both *G. bulloides* d'Orbigny, 1826 and *G. falconensis* Blow, 1959; finally, the *Globigerinoides* gr. includes all the *Globigerinoides* and *Trilobatus* specimens. The coiling ratio of *Neogloboquadrina acostaensis* (Blow, 1959) was calculated, as it is relevant for the Zanclean biozonation (Lirer et al. 2019).

Calcareous nannoplankton analysis involved the preparation of 24 smear slides using the standard method outlined in Bown & Young (1998). The slides were then observed under an optical microscope (Olympus BX50) at high magnification (1250 X), counting at least 500 nannofossils per sample.

The abundances of very rare, selected taxa (*Discoaster* spp., *Amaurolithus* and *Ceratholithus* spp.) were determined by counting a surface area of 8 mm^2 on each slide. The preservation of discoasterid specimens was poor, showing fragmentation and etching features, which in some cases hampered the taxonomic identification at the species level; for this reason, the poorly preserved specimens were counted by only differentiating the number of arms (i.e. 5-rayed and 6-rayed). In this study, taxonomic assignments are based on Perch-Nielsen (1985), Young (1998), and Nannotax (Young et al. 2022). The age model was defined according to the Mediterranean biostratigraphic zonation for the lowermost Zanclean (Di Stefano & Sturiale 2010; Di Stefano et al. 2023).

Statistical analysis

Cluster analysis. To describe the variation of the micropaleontological assemblage trough time, we conducted the clustering of samples based on the combined PF and CN micropaleontological composition. We used the hk-means algorithm implemented in the factoextra 1.0.7 R-package (http://www.R-project.org/), which combines hierarchical and k-means clustering. We included in the analysis only those PF and CN data from samples that were collected in the same stratigraphic levels (Fig. 2A).

To evaluate the effectiveness of the hk-means clustering, we determined the optimal number of clusters by WSS based elbow point method.

Principal Component Analysis. We performed the Principal Component Analysis (PCA) on the same samples used for the cluster analysis, using the `factoextra` package (version 1.0.7) in R environment (http://www.R-project.org/). The PCA is aimed at simplifying the dataset and it is used to find out the main component of paleoenvironmental variability. Indeed, this technique transforms the original dataset (made of numerous species and their percentage variation through studied stratigraphic section) into a new set of linearly uncorrelated variables known as principal components (PC), which maximize the variance. The number of significant PC is chosen through a Monte Carlo test considering the variance explained by each principal component against that of a random dataset (Fig. S1A) The scores of each principal component can be represented furthermore in a Cartesian bi-dimensional or tri-dimensional space, either plotted against stratigraphic depth or plotted one component versus another (Figs. S1B and C; Fig. S2).

Magnetostratigraphy

A total of 19 samples were drilled and oriented *in-situ* from the base to the top of the section and analyzed at the CIMaN-ALP laboratory (Peveragno, Italy). For each core, two cylindrical standard-size specimens (diameter and height of 2.5 cm) were cut. The remanent magnetization of each specimen was measured at the CIMaN-ALP laboratory using a spinner JR5 magnetometer (AGICO sro). Specimens from the same core were therefore systematically demagnetized using the thermal demagnetization (Schonstedt furnace) and alternating field (Af) demagnetization (D-2000 ASC demagnetizer).

Results

Planktic foraminifera

PF of the AAF is well-preserved and the assemblages are well-diversified and display large abundance fluctuations (Fig. 3).

The PF assemblage (Fig. b3) is mainly composed of the *Globoturborotalita* gr. showing quite regular oscillation between 18.33% and 62.74%. *N. acostaensis* has variable abundances in the lower portion of the section (up to 5.5 m), ranging from absent to maxima of 32.08%; above 5.5 m it is quite constant around 20% and then it decreases above 7

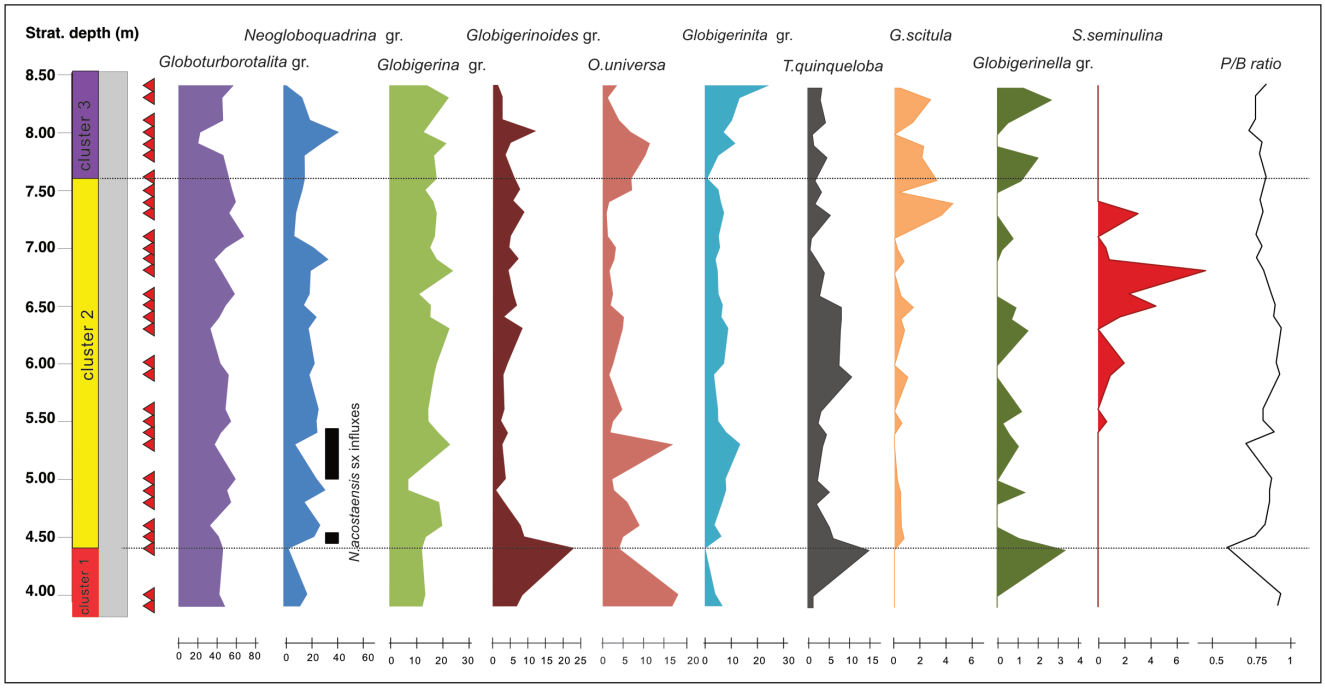

Fig. 3 - Plots of the relative abundance of planktic foraminifer taxa expressed as % of the total assemblage and of the P/B ratio of the Pollenzo section.

m up to the top of the section, except for a single increment at 8.1 m (Fig. 3). *N. acostaensis* is normally prevalently right coiled except for two left influxes at 4.50 m, and between 5.00 and 5.40 m, respectively. Apart from the basal AAF sample, where it reaches ca. 30%, the *Globigerina* gr. shows oscillations between 6.74% and 27.96%, in antiphase with the *Globoturborotalita* gr. (Fig. 3). The *Globigerinoides* gr. generally shows low abundances (usually <10%), except for the lower meter of the AAF, where it retains maximum abundances up to 23.23%. *Orbulina universa* is more abundant in the lower part of the AAF, with fluctuations between ca. 3.87 and 16.67% up to 5.30 m and then it decreases below 5%, except a 11.25% peak at 7.9 m. The *Globigerinita* gr. is also relatively scarce (<5%), increasing above 5% only in two intervals between 4.25 and 5.25 m and in the topmost 60 cm (Fig. 3). The remaining taxa occur with lower abundances (Fig. 3), including a) *Turborotalita quinqueloba* (Natland, 1938), which decreases upward, ranging from a maximum of 12.26% to a minimum of 0.47%; b) *Globorotalia scitula* (Brady, 1882) , absent in the lower part of the section and gradually increasing up to a maximum of 4.15% in the upper part; c) *Globigerinella* spp., discontinuously present with maximum relative abundances of 3.23% and d) *Sphaeroidinellopsis seminulina* (Schwager, 1866) only present between 5.5 and 7.5 m, with maxima below 5% (see also supplementary table ST1).

Calcareous nannofossils

The CN assemblage (Fig. 4) is characterized by high abundance of the *Reticulofenestra* gr. *Reticulofenestra minuta* Roth, 1970 dominates the assemblage with an increasing abundance trend up to the top (up to 57.91% at 7.80 m; Table ST1); *Reticulofenestra haqii* Backman, 1978 shows maxima at 5.00 m (16.8%), 7.50 m (8.85%) and 8.00 m (9.43%); *Umbilicosphaera jafari* Muller, 1974 depicts a decreasing upward trend with slight fluctuations in abundance ranging between 19.40% at 3.90 m and 0.98% at 8.00 m. *Reticulofenestra zancleana* Di Stefano & Sturiale, 2010 has its highest abundance at the base of the AAF at 3.90 m (8.8%) and rapidly declines upwards (below 2% from 4.40 m); it is continuously present up to 5.30 m and upward is irregularly present with relative abundances below 1%. *Helicosphaera carteri* (Wallich, 1877) is common (with a prominent peak of 21.4% at 4.60 m) in the lower part of the section, up to 5.00 m, and it decreases below 7% above 6.5 m (Fig. 4). *Sphenolithus abies* Deflandre & Fert, 1954 shows maxima in abundance between 5 and 6.25 m (up to ca. 10%), otherwise it does not exceed 5%. *Calcidiscus leptoporus* (Murray & Blackman, 1898) shows two abundance peaks at 4.00 m (12%) and 6.00 m (9.2%), with a

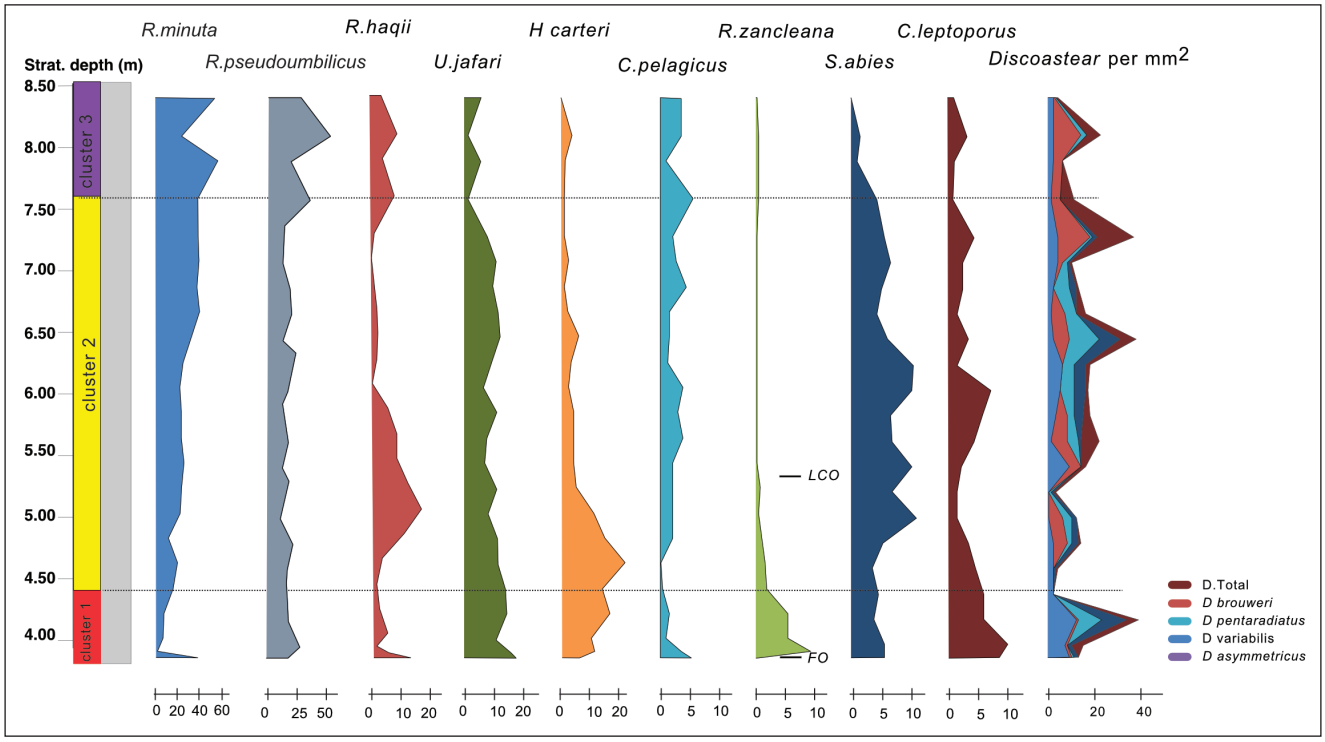

Fig. 4 - Plots of the relative abundance of calcareous nannofossil taxa, expressed as % of the total assemblage. FO and LCO are first occurrence and last common occurrence for *R. zancleana*.

pronounced drop in between; from 6.00 m to the top of the section it remains below 5% (Fig. 4). *Coccolithus pelagicus* (Wallich, 1877) shows minor fluctuation with maxima lower than 5%, except for a prominent peak at very base of the AAF (9.0%). Minor components of the assemblage are *Rhabdosphaera clavigera* Murray & Blackman, 1898, *Umbilicosphaera rotula* (Kamptner, 1956), and *Pontosphaera* spp.; very rare taxa are *Scyphosphaera lagena* Kamptner, 1955, *Syracosphaera pulchra* Lohmann, 1902, *Amaurolithus primus* (Bukry & Percival, 1971); *Ceratholithus acutus* Gartner & Bukry, 1974 occurs from the base of the AAF and is overall extremely rare. Additionally, the association is characterized by the scattered occurrences of different species of *Discoaster* (*D. variabilis* gr., *D. brouweri* gr., *D. pentaradiatus* gr., together with poorly preserved *D.* 5 arms, *D.* 6 arms). The abundance of *Discoaster* spp. per mm^2 varies with a regular and cyclical pattern, with maxima at 4.20 m (39/mm^2), 4.80 m (14/mm^2), 5.60m (22/mm^2), 6.40 m (38/mm^2), 7.20 m (37/mm^2), and at 8.0 m (22/mm^2), and minima at 4.40 m, 5.20 m, 6.00 m and 7.00 m, and 7.80 m (Table ST1c).

Cluster analysis

According to the within sum of squares (WSS) and the elbow point method, three clusters were defined based on the PF and CN assemblages (Figs. 5A and B). The silhouette score was used as a criterion to evaluate the distribution of the assemblages within the clusters (Fig. 5C), as, in our case, it measures the similarity of an assemblage to its assigned cluster compared to other clusters. A high silhouette score indicates that the assemblage fits well within its own cluster. All the samples except MP2c and 2d display positive values, and the three clusters are arranged in stratigraphic order (Fig. 5A).

Cluster 1 comprises samples of the bottommost portion of the AAF, ranging from 3.90 to 4.40 m. The mean assemblage of Cluster 1 (Fig. S3) is characterized by *Reticulofenestra pseudoumbilicus* (Gartner, 1967) (20%), *R. minuta* (7%) and *R. haqii* (5%), and, with significant contributors being *C. pelagicus* (3%), *H. carteri* (13%), and *U. jafari* (17%), among CN. Regarding PF, the dominant species include *Globoturborotalita* spp. (42%), *Globigerina spp.* (12%), and *Neogloboquadrina acostaensis* (dx) (10%).

Cluster 2 (Fig. S3) includes samples from the intermediate part of the AAF, spanning from 4.50 to 7.50 m. Among CN, the main changes respect to Cluster 1 are represented by *R. minuta* (28%), *R. pseudoumbilicus* (17%), *U. jafari* (12%) and *H. carteri* (7%); *R. zancleana* is absent and other taxa remain roughly unchanged. Regarding PF, *Globoturborotalita*

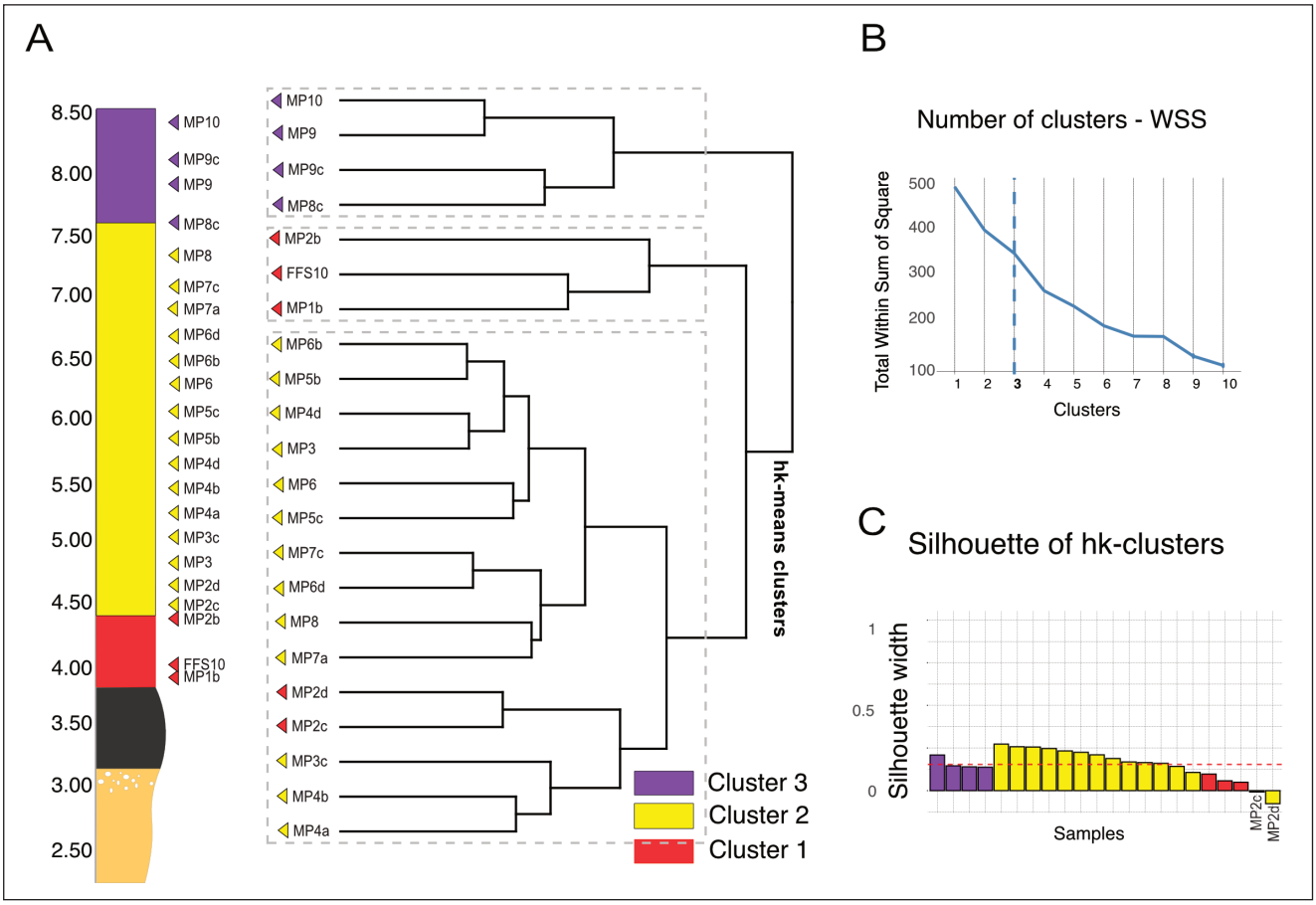

Fig. 5 - A) Hk-means cluster analyses on calcareous nannofossils and planktic foraminifers and their stratigraphic distribution; B) the WSS plot with the variance explained by the corresponding number of clusters; C) silhouette scores plot for hk-means; each bar represents a sample; the red dotted line indicates the silhouette mean value and colors of the bars indicate clusters.

spp. remains prominent (44%), there is an uptick in *Globigerina* spp. (16%) and *Globigerinita* spp. (6%). Notably, *N. acostaensis* (dx) maintains a substantial presence (15%).

Cluster 3 (Fig. S3) represents the topmost portion of the section, extending from 7.50 m to the top (Fig. 5A). Notably, *R. minuta* experiences a substantial increase in abundance (45%), becoming the dominant species within the cluster. Similarly, *R. pseudoumbilicus* exhibits a marked rise in relative abundance (31%). In contrast, several species witness declines, including *H. carteri* (3%), *S. abies* (3%), and *U. jafari* (4%). In Cluster 3 the mean assemblage is still mainly made up of *Globoturborotalita* (40%), *N. acostaensis* dx (18%) and *Globigerina* spp. (16%), while *Globigerinita* spp. increase; other taxa remain unchanged.

Principal component analysis

The PCA test, validated through a Monte Carlo test (Fig. S1A), identifies three principal components: PC1, PC2, and PC3, which account for 23.12%, 14% and 12% of the variance, respectively.

The distribution of the samples in the PC1-PC2 plane biplot (Fig. S1C) reflects the clustering patterns, particularly for cluster 1. In fact, species that are well represented in samples of cluster 1, such as *R. minuta*, *R. haqii*, *R. pseudoumbilicus*, *C. pelagicus*, *G. scitula*, *Globigerina* spp., *Globigerinita* spp., *Neogloboquadrina dutertrei, O. universa,* and *Sphaeroidinellopsis* spp. contribute positively to PC1 (Fig. S1C). Conversely, species like *R. zancleana*, *H. carteri*, *S. abies*, *C. leptoporus*, *Discoaster* spp., *U. rotula*, *U. jafari*, *R. clavigera*, *P. japonica*, *P. discopora*, *P. multipora*, *S. pulchra*, *Globigerinoides* spp., *Globigerinella* spp., *N. acostaensis* sx, and *Globoturborotalita* spp. contribute negatively (Fig. S1C).

For PC2, species such as *R. pseudoumbilicus*, *Globigerinoides* spp., *Neogloboquadrina* dx, and *O. universa* contribute positively (Fig. S1C), while *R. zancleana*, *C. leptoporus*, *P. japonica*, *S. pulchra*, *G. scitula*, *Globigerina* spp., *Globigerinita* spp., *N. acostaensis* sx,

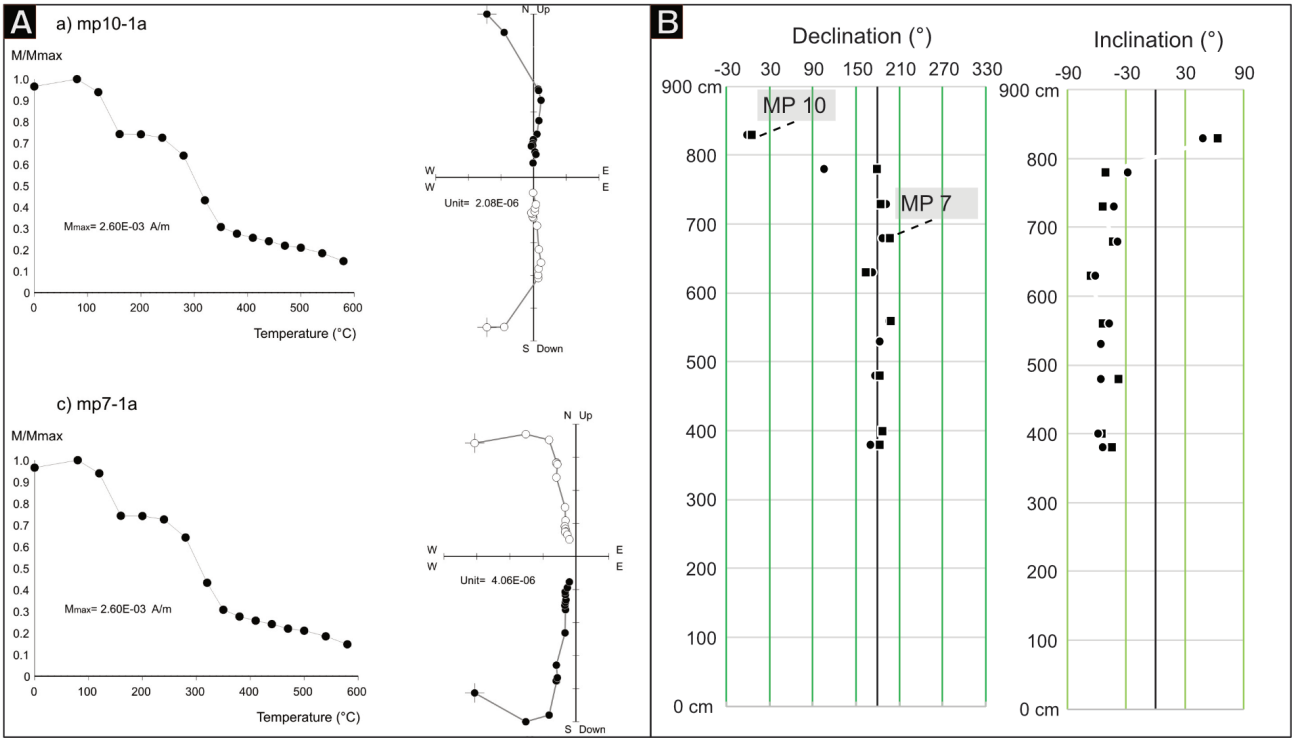

Fig. 6 - A) Zijderveld diagrams: demagnetization data on normal specimen (MP10) and reverse specimen (MP7). (a) and (c) are thermal demagnetization. From the left, the plot of the normalized magnetization intensity as a function of the applied thermal/field steps, the Zijderveld diagram (full/open dot = declination/apparent inclination); B) stratigraphic variation of declination and inclination (dot=alternate field, square=thermal demagnetized data).

Globoturborotalita spp., *T. quinqueloba*, and *Sphaeroidinellopsis* spp. contribute negatively (Fig. S1C).

Stratigraphically, the PC1 exhibits a significant gradual trend upward from negative to positive values; PC2 shows positive scores in the intervals corresponding to clusters 1 and 3; PC3 shows no clear trends (Fig. S1B, Fig. S2A, B). In term of scores, there is a striking difference between PC1 and 2 in the basal portion of the section, corresponding to samples of cluster 1; upward this difference is less evident.

Magnetostratigraphy

The analysis of the Zijderveld diagrams (Fig. 6A), shows that both the thermic and AF demagnetizations are characterized by two clearly defined magnetization directions. The low-stability direction, which is identified up to 10-20 mT and 120-160 °C range, is interpreted as a viscous component (VRM).

At higher field and temperatures, the characteristic remnant magnetization (ChRM) is always well-defined in all the samples and shows both normal and reversed polarities. The samples from MP1 to MP9 (7.60 m) exhibit reverse polarity (n = 16, D = 13.5°, I = -49.6°, k = 7, α_{95} = 4.7°), while sample MP10 (8.50 m) has normal polarity (n = 2, D = 1.0°, I = 48.3°) (Fig. 6B).

Discussion

Biomagnetostratigraphy and age model

The CN and PF assemblages allow the identification of the biozones reported by Di Stefano et al. (2023) and by Lirer et al. (2019) for the earliest Pliocene. In particular, as displayed in Fig. 7B, the occurrences of two influxes of left coiled *N. acostaensis*, the acme of *S. seminulina* (Fig. 7B) and the absence of *Globorotalia margaritae* allow to refer the whole studied section to the MPL1 PF biozone (Fig. 7B; Iaccarino et al. 1999; Gennari et al. 2008).

The first occurrence of *R. zancleana* in the lowermost sample of the AAF at 3.90 m provides a reliable marker for the beginning of the Zanclean at 5.33 Ma (Fig. 7A, B), marking the base of the MNN12a CN biozone (Di Stefano et al. 2023). We placed the LCO of *R. zancleana* at 5.35 m, where this taxon become very rare and discontinuously

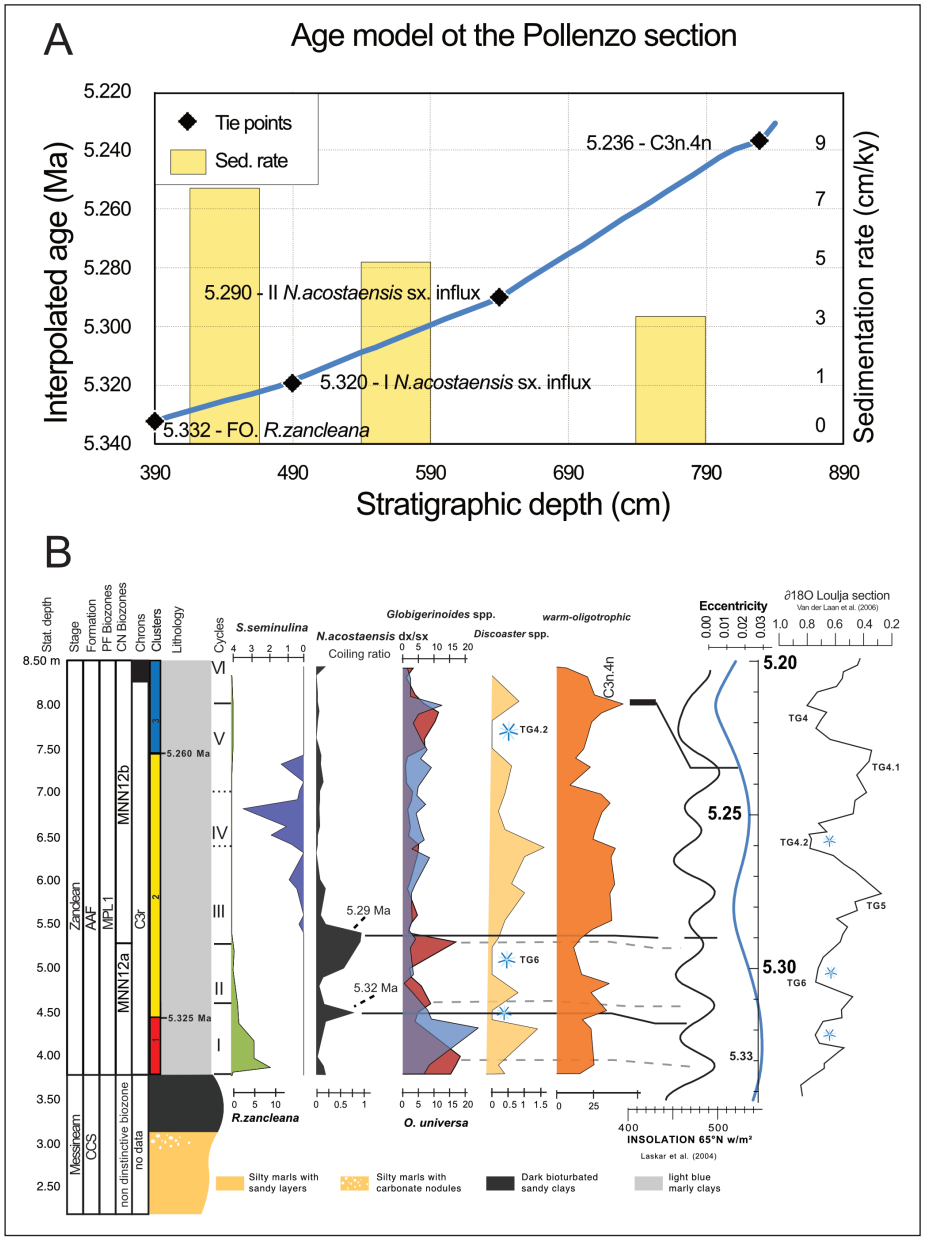

Fig. 7 - A) Age model of the Pollenzo section based on tie points and the sedimentation rate in cm/ky; B) the biomagnetostratigraphic age model of the Pollenzo section. Insolation from Laskar et al. 2004 and $\delta^{18}O$ from Van der Laan et al. (2006); blue asterisks indicate cold climate intervals; CN biozone are reported from Di Stefano et al. (2023) considering the constrained cycles and our age model; TG labels are referred to marine glacial stages. Insolation and eccentricity are from Laskar et al. (2004).

present; this stratigraphic level corresponds to the boundary between the MNN12a and the MNN12b biozones. The rare occurrence of *C. acutus* further supports the early Zanclean age for the base of the section (Raffi et al. 2020; Di Stefano et al. 2023). Consequently, the polarity reversal placed at the midpoint (8.05 m) between the uppermost reversed sample at 7.8 m and the lowermost normal sample at 8.3 m (Fig. 7B) is interpreted as the base of the Thvera subchron (C3n.4n), dated at 5.236 Ma (Hilgen & Langereis 1988; Gradstein et al. 2020), which occurs 5 precessional cycles above the MZB in the Eraclea Minoa reference section (Van Couvering et al. 2000). Other than the magnetic reversal, also the PF bioevents were astronomically dated and can be used as tie points for the reconstruction of the age model (Fig. 7A), performed with an R script available on GitHub (https://github.com/NewGeoProjects/Speck_Trial). The two influxes of sinistral-coiling *N. acostaensis* (Lirer et al. 2019) are dated at 5.29 Ma (sample MP2c at 4.50 m) and 5.31 Ma (sample MP4b at 5.40 m), respectively (Fig. 7A, B); in the Capo Rossello and Eraclea Minoa sections they occur at the base of the second and third precessional cycles above the MZB (Fig. 7; Iaccarino et al. 1999).

According to the age model, the age of the *S. seminulina* acme and of the FCO of *R. zancleana* in the Pollenzo section are diachronous with respect to the Mediterranean reference sections. The *S. sem-*

inulina acme starts at 5.30 and ends at 5.21 Ma (Lirer et al. 2019); however, Gennari et al. (2008) showed that its duration is often reduced in the Northern Mediterranean, probably due to depth preference of this taxon (Aze et al. 2011). The shorter duration is also observed in the Pollenzo section (Fig. 7B), where the acme basis postdates the 1st influx of left coiled *N. acostaensis* (5.29 Ma) and the acme end predates the Thvera base (5.23 Ma).

It is worth noting that the short stratigraphic interval spanning from the FO and the LCO of *R. zancleana* (below the 2nd left coiled *N. acostaensis* influx) does not correspond to the full distribution range of this taxon as recorded in other sections in the Mediterranean located at lower latitudes (Di Stefano et al. 2023), where the LCO occurs in the 7th cycle above the Zanclean base. Another CN bioevent lacking at Pollenzo is the paracme base of *R. pseudoumbilicus*, which is reported to be slightly diachronous in the Mediterranean, ranging from cycle 2 to 6 (Di Stefano & Sturiale 2010) from the MZB. In the Northern Apennine this event occurs in cycle 6 and it is possible that our record is too old to pick it up; however, we also note that the distribution of this taxon is more continuous and characterized by higher relative abundances with respect, for example, to the Montepetra borehole in the Marche region (Gennari et al. 2008; Di Stefano & Sturiale 2010). Regarding PF, the duration of the *S. seminulina* (a tropical and deep thermocline dweller according to Aze et al. 2011) acme is shorter (cycles 3 to 5) than in the reference sections of the Southern Mediterranean (Iaccarino et al. 1999), where it lasted from cycles 2 to 6. This was also observed in other Northern Mediterranean successions (Gennari et al. 2008) and we speculate that the optimal conditions for this taxon were not met in the Northern part of the Mediterranean. These biostratigraphic differences could be related to the peculiar paleoenvironment of the Piedmont Basin or to the northern position and the consequent paleoclimatic differences with the reference sections. This aspect needs to be further investigated in other northern Mediterranean successions.

The influence of orbital forcing on CN and PF

In the Pollenzo section, the monotonous lithology of the AAF hinders the recognition of the lithological cycles; however, it is still possible to recognize the influence of variation of orbital parameters on the distribution of the calcareous plankton assemblage (Figs. 7A, B). Peaks of the warm/oligotrophic (WO) PF taxa have associated to insolation maxima in the pre-MSC successions of the Mediterranean basin (Sierro et al. 2003; Rouchy et al. 2001; Lozar et al. 2010; Gennari et al. 2018), where they reflect warming sea surface temperature (SST) and stratification (Hilgen & Krijgsman 1999; Sierro et al. 2001; Kouwenhoven et al. 2006; Gennari et al. 2018, 2020; Lozar et al. 2018; Mancini et al. 2020). In the Sorbas succession *O. universa* is the main contributor of the WO group (Sierro et al. 2003). In the Zanclean deposits, the fluctuations of *Globigerinoides* spp. were instead commonly used to recognize precession driven cycles (Iaccarino et al. 1999). In the Pollenzo section, the WO group is largely dominated by the *Globoturborotalita* gr., whilst *Globigerinoides* gr. and *O. universa* are subordinated, except in the lower part of the AAF. However, the WO group does not show any regular abundance fluctuations (Fig. 7B). Instead, in the lower portion of the AAF the WO taxon *O. universa* shows three abundance peaks which, combined with the position of the 1st and 2nd peak of left coiling *N. acostaensis* (top 1st/base 2nd and base 3rd precessional cycle above the MZB, respectively), suggest that this species is favored during insolation maxima phases, when SST warmed and triggered stratification (Fig. 7B). The abundance pattern of *O. universa* in the Pollenzo section is consistent with that of the *Globigerinoides* group in southern Mediterranean sections (Iaccarino et al. 1999).

In fact, above 5.5 m and up to 7.5 m (Fig. 7B), *O. universa* decreases and loses its cyclical pattern up to the abundance peak recorded close to the base of the Thvera subchron, a feature also observed for the *Globigerinoides* gr. (Fig. 7B) in southern Mediterranean successions (Iaccarino et al. 1999; Gennari et al. 2008). The pattern of these species is probably due to a 400 Ka eccentricity minimum which contribute to reduce the amplitude of the insolation maxima (Laskar et al. 2004) and their influence on paleoceanographic conditions, preventing notable SST warming.

Among CN, the abundance of the deep photic zone dwellers *Discoaster* spp. was correlated with obliquity in the low latitude open ocean (Gibbs et al. 2004) and with insolation in the Mediterranean

pre-MSC succession of the Sorbas basin, when warming of the sea surface promotes the formation of a deep pycnocline (Flores et al. 2005). In our section, the *Discoaster* spp. gr. is rare; however, compared with the oceanic $\delta^{18}O$ curve of Van der Laan et al. (2006), it can be noted that its absence matches well the peaks of relatively heavier isotopic values, corresponding to the marine isotopic glacial stages TG6 and TG4.2 (Fig. 7B) or to cooler climatic phases. Conversely, the increments are in phase with warmer climate, following a cyclic pattern influenced by insolation (in the lower portion of the AAF) and obliquity (in the middle-upper part, TG5 and TG4.1 base).

Environmental evolution and marine transition in the Northern Mediterranean Post-MSC: evidence from the Pollenzo section

The return to open marine conditions following the demise of the MSC is a topic of intense debate (see Andreetto et al. 2021, 2022 for a comprehensive review). Recently, Pilade et al. (2023) proposed a gradual restoration of open marine conditions in the Northern Mediterranean. In this context, the Pollenzo sector within the Piedmont Basin was identified as a shallow and proximal-coastal area during the latest phase of the MSC (Andreetto et al. 2022b). Unlike the more distal and southern Maccarone section (Caloni et al. 1974); Bertini et al. 2006, 2011), where the marine transgression exhibits transitional characteristics, at Pollenzo, the influx of marine water occurred abruptly and coincided with the Zanclean base (Pilade et al. 2023). Thus, the modality of the demise of the MSC seems to be linked to the different environmental setting and is not homogeneous over the Mediterranean area. Does the marine Zanclean deposits record these different modalities? In the Maccarone section (Gennari et al. 2008), the demise occurred in a relatively deep water setting and this is also testified by the few benthic foraminifera, typical of a bathyal paleodepth, retrieved in the basal Zanclean deposits, similar to other successions in the central Mediterranean (Iaccarino et al. 1999). In the Pollenzo section the cluster analysis help identify three intervals (Fig. 5; Fig. S1B; Fig. S2), that, along with the trends from negative to positive scores observed on PC1 (Fig. S1B; Fig. S2) suggest an environmental evolution following the reestablishment of marine conditions above the MZB.

The basal Cluster 1, roughly corresponding to the first precessional cycle spanning an age range from approximately 5.33 Ma to 5.32 Ma (Fig. 7B), is characterized by the calcareous nannofossil *H. carteri* (Fig. S3). Although not dominant, this species is characteristic of Cluster 1 and progressively became subordinated in clusters 2 and 3. *H. carteri* is an extant species known to thrive in mesotrophic/eutrophic, hyposaline, and turbid waters (Ziveri et al. 2004), as well as in estuarine and coastal environments (Cachão et al. 2002; Dimiza et al. 2014; Bonomo et al. 2017). Typically inhabiting the mid-photic zone (Corselli et al. 2002), *H. carteri* also favors warm and mesotrophic waters (Ziveri et al. 2004; Mancini et al. 2021). Its abundance in Cluster 1 can reflect the runoff influence in a marine setting relatively close to the coast, as inherited from the latest phase of the MSC. The runoff influences could had contributed to a nutrient increase, which also explain the abundance of *U. jafari* in Cluster 1. In other Mediterranean successions the occurrence of *H. carteri* was not noted, although Di Stefano and Sturiale (2010) indicate and that this species is the dominant helicolith at sites 969B and 975B; conversely, the same authors found high proportion of another helicolith (*H. intermedia*) in the 1st cycle above the MZB at Montepetra (Northern Apennine).

Cluster 2 and 3, covering an age range from approximately 5.32 to 5.25 Ma (cycles 2 to 5) and 5.25 Ma to 5.23 Ma (Fig. 7B), respectively, mark a progressive and gradual decrease of *H. carteri* and *U. jafari*, replaced by *R. minuta* (Fig. 4, Fig. S3), an opportunistic taxon inhabiting the upper water column, adapted to more open marine and high nutrient conditions (Athanasiou et al. 2015; Auer et al. 2014; Flores et al. 1995; Imai et al. 2015; Takahashi & Okada 2000; Mancini et al. 2021) and to changes in salinity (Wade & Bown 2006). This change is coupled with the gradual increase of the deep dweller PF *G. scitula* (absent in Cluster 1; Fig. 3), typically found in modern subsurface pelagic waters at depths of 200–300 meters (Schiebel & Hemleben 2017). Another relatively deep dweller PF (living at the thermocline according to Aze et al. 2011) that increase in frequency from Cluster 1 to 3 (from 11 to 19%) is *N. acostaensis*.

These changes in the cluster composition parallel the PC1 that increases from negative to positive scores from the Cluster 1 to 3 interval. In fact, the taxa considered as proxy of more open marine conditions positively score on PC1.

The multivariate analysis, along with the slowdown of the sedimentation rate (Fig. 7A) and the increase of the P/B ratio (Fig. 3), suggests a significant environmental change between 5.32 and 5.25 Ma (Cluster 2). During this period, the relatively more proximal environment characterizing the 1st Zanclean insolation cycle (Cluster 1) in Pollenzo transitioned into a more open sea environment. This transformation, which occurred after 5.25 Ma (Cluster 3), followed the trend of rising sea levels that began in the latest Messinian. A similar trend was also observed in the Sorbas Basin (Western Mediterranean), where a basal Zanclean coastal plain evolved into a bay/lagoon and then into an open marine environment below the Thvera base (Roveri et al. 2019).

As for PC2 and 3, their interpretation is less straightforward. Positive PC2 scores seems to indicate warmer conditions (*Globigerinoides* spp., *O. universa*, *Discoaster* spp.) as opposed to the cooler *Globigerina* genus. However, the overall availability of nutrient and preys, and their surface to intermediate water distribution may complicate the interpretation of environmental gradient on the PC axis (see also Azibeiro et al. 2023; Mancini et al. 2024). Finally, the precessional oscillation of oceanographic conditions, not completely constrained due to a low sampling resolution, could have further hindered a clear subdivision of taxa on the PCA.

Conclusion

Through biomagnetostratigraphy and cyclostratigraphy of the Pollenzo section, we have unraveled significant insights into the environmental evolution of the northernmost Mediterranean region at the Messinian-Zanclean transition. Our investigation suggests extending the synchronicity of the return to marine conditions following the MSC to the northernmost part of the Mediterranean. This is recognized thanks to the identification of the two influxes of *N. acostaensis* sx and the pattern of *O. universa*, which was correlated to insolation maxima, that define the lowermost two Zanclean precessional cycles.

Multivariate analysis highlights the peculiar distribution of CN and PF taxa that is indicative of runoff influence during the 1st precessional Zanclean cycle, and of a gradual transition from relatively more coastal to more open marine conditions from cycle 2 to 6. This trend seems to be peculiar of the Pollenzo section and due to its marginal position, as inherited from the latest MSC phase (Lago-Mare), that differentiates this section from most of the Mediterranean reference sections and boreholes.

References

Amarathunga U., Hogg A.M., Rohling E.J., Roberts A.P., Grant K.M., Heslop D., Hu P., Liebr D., Westerhold T., Zhao X. & Gilmore S. (2022) - Sill-controlled salinity contrasts followed post-Messinian flooding of the Mediterranean. *Nature Geosciences*, 15(9): 720-725.

Andreetto F., Aloisi G., Raad F., Heida H., Flecker R., Agiadi K., Lofi J., Blondel S., Bulian F., Camerlenghi A. & Caruso A. (2021) - Freshening of the Mediterranean Salt Giant: controversies & certainties around the terminal (Upper Gypsum & Lago-Mare) phases of the Messinian Salinity Crisis. *Earth Sciences Review*, 216: 103577.

Andreetto F., Mancini A.M., Flecker R., Gennari R., Lewis J., Lozar F., Natalicchio M., Sangiorgi F., Stoica M., Dela Pierre F. & Krijgsman W. (2022) - Multi-proxy investigation of the post-evaporitic succession of the Piedmont Basin (Pollenzo section, NW Italy): a new piece in the stage 3 puzzle of the Messinian Salinity Crisis. *Palaeogeography, Palaeoclimatology, Palaeoecology*, 594: 110961.

Andreetto F., Mancini A.M., Flecker R., Gennari R., Lewis J., Lozar F., Natalicchio M., Sangiorgi F., Stoica M., Pierre F.D. & Krijgsman W. (2022b) - Multi-proxy investigation of the post-evaporitic succession of the Piedmont Basin (Pollenzo section, NW Italy): A new piece in the Stage 3 puzzle of the Messinian Salinity Crisis. *Palaeogeography, Palaeoclimatology, Palaeoecology*, 594: 110961.

Athanasiou M., Triantaphyllou M.V., Dimiza M.D., Gogou A. & Theodorou G. (2015) - Zanclean/Piacenzian transition on Cyprus (SE Mediterranean): calcareous nannofossil evidence of sapropel formation. *Geo-Marine Letters*, 35: 367-385.

Auer G., Piller W.E. & Harzhauser M. (2014) - High-resolution calcareous nannoplankton palaeoecology as a proxy for small-scale environmental changes in the Early Miocene. *Marine Micropaleontology*, 111: 53-65.

Aze T., Ezard T.H., Purvis A., Coxall H.K., Stewart D.R., Wade B.S. & Pearson P.N. (2011) - A phylogeny of Cenozoic macroperforate planktonic foraminifera from fossil data. *Biological Reviews*, 86(4): 900-927.

Bertini A. (2006) - The Northern Apennines palynological record as a contribute for the reconstruction of the Messinian palaeoenvironments. *Sedimentary geology*, 188: 235-258.

Azibeiro L.A., Kučera M., Jonkers L., Cloke-Hayes A., Sierro F.J. (2023) - Nutrients and hydrography explain the composition of recent Mediterranean planktonic foraminiferal assemblages. *Marine Micropaleontology*, 179: 102201.

Bertini A. & Martinetto E. (2011) - Reconstruction of vegetation transects for the Messinian–Piacenzian of Italy by means of comparative analysis of pollen, leaf and carpological records. *Palaeogeography, Palaeoclimatology, Palaeoecology*, 304(3-4): 230-246.

Blanc-Valleron M.M., Pierre C., Caulet J.P., Caruso A., Rouchy

J.M., Cespuglio G., Sprovieri R., Pestrea S. & Di Stefano E. (2002) - Sedimentary, stable isotope and micropaleontological records of paleoceanographic change in the Messinian Tripoli Formation (Sicily, Italy). *Palaeogeography, Palaeoclimatology, Palaeoecology*, 185(3-4): 255-286.

Bonomo S., Placenti F., Quinci E.M., Cuttitta A., Genovese S., Mazzola S. & Bonanno A. (2017) - Living coccolithophores community from southern Tyrrhenian Sea (Central Mediterranean-summer 2009). *Marine Micropaleontology*, 131: 10-24.

Bown P.R. & Young J.R. (1998) - Techniques. In: Bown P. (Ed.) - Calcareous Nannofossil Biostratigraphy. British Micropalaeontology Society Publications Series, Cambridge: Kluwer Academic Publisher: 16-28.

Bulian F., Kouwenhoven T.J., Andersen N., Krijgsman W. & Sierro F.J. (2022a) - Reflooding and repopulation of the Mediterranean Sea after the Messinian Salinity Crisis: Benthic foraminifera assemblages and stable isotopes of Spanish basins. *Marine Micropaleontology*, 176: 102160.

Bulian F., Kouwenhoven T., Jiménez-Espejo F., Krijgsman W., Andersen N. & Sierro F. (2022b) - Impact of the Mediterranean-Atlantic connectivity and the late Miocene carbon shift on deep-sea communities in the Western Alboran Basin. *Palaeogeography, Palaeoclimatology, Palaeoecology*, 589: 110841.

Cachão M., Drago T., Silva A.D., Moita T., Oliveira A. & Naughton F. (2002) - The secret (estuarine?) life of Helicosphaera carteri: preliminary results. J*ournal of Nannoplankton Research*, 24(2): 76-77.

Carloni G.C., Francavilla F., Borsetti A.M., Cati F., D'onofrio S., Mezzetti R. & Savelli C. (1974) - Ricerche stratigrafiche sul limite Miocene – Pliocene nelle Marche centromeridionali. *Giornale di Geologia*, 39: 363-392.

Carnevale G. & Schwarzhans W. (2022) - Marine life in the Mediterranean during the Messinian salinity crisis: a paleoichthyological perspective. *Rivista Italiana di Paleontologia e Stratigrafia*, 128: 283-324.

Carnevale G., Dela Pierre F., Natalicchio M. & Walter L. (2018) - Fossil marine fishes and the 'Lago-Mare' event: has the Mediterranean ever transformed into a brackish lake? *Newsletters on Stratigraphy*, 51(1): 57-72.

Caruso A., Blanc-Valleron M.M., Da Prato S., Pierre C. & Rouchy J.M. (2020) - The late Messinian "Lago-Mare" event and the Zanclean reflooding in the Mediterranean Sea: New insights from the Cuevas del Almanzora section (Vera Basin, South-Eastern Spain). *Earth Sciences Review* 200: 102993.

Castradori D., Rio D., Hilgen F.J. & Lourens L.J. (1998) - The global standard stratotype-section and point (GSSP) of the Piacenzian Stage (Middle Pliocene). *Episodes Journal of International Geoscience*, 21(2): 88-93.

CIESM (2008) - The Messinian salinity crisis from mega-deposits to microbiology. In: Briand F. (Ed.) - A consensus report, in 33ème CIESM Workshop Monographs, 33. CIESM, 16, bd de Suisse, MC-98000, Monaco: 1-168.

Colalongo M.L. (1988) - Planktic foraminifer biostratigraphy, with remarks on benthic foraminifers and ostracodes (Monticino quarry Faenza). In: C. De Giuli & G.B. Vai (Eds.) - Fossil vertebrates in the Lamone valley, Romagna Apennines. International Workshop on Continental faunas at the Miocene-Pliocene Boundary, March 28-31, 1988, Field Trip Guidebook, Faenza: 53-54.

Colombero S., Alba D.M., D'Amico C., Delfino M., Esu D., Giuntelli P., Harzhauser M., Mazza P., Mosca M., Neubauer T.A. & Pavia G. (2017) - Late Messinian mollusks and vertebrates from Moncucco Torinese, north-western Italy. Paleoecological and paleoclimatological implications. *Palaeontologia Electronica*, 20: 1-66.

Corselli C., Principato M.S., Maffioli P. & Crudeli D. (2002) - Changes in planktonic assemblages during sapropel S5 deposition: Evidence from Urania Basin area, eastern Mediterranean. *Paleoceanography*, 17(10): 1029, 1029/2000PA000536.

Dela Pierre F., Clari P., Bernardi E., Natalicchio M., Costa E., Cavagna S., Lozar F., Lugli S., Manzi V., Roveri M. & Violanti D. (2012) - Messinian carbonate-rich beds of the Tertiary Piedmont Basin (NW Italy): microbially-mediated products straddling the onset of the salinity crisis. *Palaeogeography, Palaeoclimatology, Palaeoecology*, 344: 78-93.

Dela Pierre F., Natalicchio M., Lozar F., Bonetto S.M.R., Carnevale G., Cavagna S., Colombero S., Sabino M. & Violanti D. (2016) - The Northermost record of the Messinian salinity crisis (Piedmont Basin, NW Italy). *Geological Field Trips*, 8(21): 1-58.

Dela Pierre F., Bernardi E., Cavagna S., Clari P., Gennari R., Irace A., Lozar F., Lugli S., Manzi V., Natalicchio M. & Violanti D. (2011) - The record of the Messinian salinity crisis in the Tertiary Piedmont Basin (NW Italy): the Alba section revisited. *Palaeogeography, Palaeoclimatology, Palaeoecology*, 310(3-4): 238-255.

Di Stefano A. & Sturiale G. (2010) - Refinements of calcareous nannofossil biostratigraphy at the Miocene/Pliocene Boundary in the Mediterranean region. *Geobios* 43(1): 5-20.

Di Stefano A., Baldassini N., Raffi I., Fornaciari E., Incarbona A., Negri A., Bonomo S., Villa G., Di Stefano E. & Rio D. (2023) - Neogene-Quaternary Mediterranean calcareous nannofossil biozonation and biochronology: A review. *Stratigraphy*, 20(4): 259-302.

Di Stefano E., Sprovieri R. & Scarantino S. (1996) - Chronology of biostratigraphic events at the base of the Pliocene. *Palaeopelagos*, 6: 401-414.

Dimiza M.D., Triantaphyllou M.V. & Malinverno E. (2014) - New evidence for the ecology of Helicosphaera carteri in polluted coastal environments (Elefsis Bay, Saronikos Gulf, Greece). *Journal of Nannoplankton Research*, 34: 37-43.

Flores J.A., Sierro F.J. & Raffi I. (1995) - Evolution of the calcareous nannofossil assemblage as a response to the paleoceanographic changes in the eastern equatorial Pacific Ocean from 4 to 2 Ma (Leg 138, Sites 849 and 852). In: Proceedings of the Ocean Drilling Program, Scientific Results (Vol. 138, pp. 163-176). Ocean Drilling Program College Station, TX.

Flores J.A., Sierro F.J., Filippelli G.M., Bárcena M.Á., Pérez-Folgado M., Vázquez A. & Utrilla R. (2005) - Surface water dynamics and phytoplankton communities during deposition of cyclic late Messinian sapropel sequences in the western Mediterranean. *Marine Micropaleontology*, 56(1-2): 50-79.

Garcia-Castellanos D., Estrada F., Jiménez-Munt I., Gorini C., Fernández M., Vergés J. & De Vicente R. (2009) - Catastrophic flood of the Mediterranean after the Messinian salinity crisis. *Nature*, 462(7274): 778-781.

García-Alix A., Minwer-Barakat R., Martin Suarez E., Freudenthal M., Aguirre J. & Kaya F. (2016) - Updating the Europe–Africa small mammal exchange during the late Messinian. *Journal of Biogeography*, 43(7): 1336-1348.

Gennari R., Iaccarino S.M., Di Stefano A., Sturiale G., Cipollari P., Manzi V., Roveri M. & Cosentino D. (2008) - The Messinian–Zanclean boundary in the Northern Apennine. *Stratigraphy*, 5(3-4): 309-325.

Gennari R., Lozar F.M.J., Natalicchio M., Zanella E., Carnevale G. & Dela Pierre F. (2020) - Chronology of the Messinian events in the northernmost part of the Mediterranean: The Govone section (Piedmont Basin, NW Italy). *Rivista Italiana di Paleontologia e Stratigrafia*, 126(2): 541-560.

Gennari R., Lozar F., Turco E., Dela Pierre F., Lugli S., Manzi V., Natalicchio M., Roveri M., Schreiber B.C. & Taviani M. (2018) - Integrated stratigraphy and paleoceanographic evolution of the pre-evaporitic phase of the Messinian salinity crisis in the Eastern Mediterranean as recorded in the Tokhni section (Cyprus island). *Newsletter on Stratigraphy*, 52(1): 33-55.

Ghielmi M., Serafini G., Artoni A., Di Celma C. & Pitts A. (2019) - From Messinian to Pleistocene: tectonic evolution and stratigraphic architecture of the central Adriatic foredeep (Abruzzo and Marche, Central Italy). In: Field Trips-Guide Book: 53-91. Associazione Italiana di Geologia del Sedimentario-GeoSed.

Gibbs S., Shackleton N. & Young J. (2004) - Orbitally forced climate signals in mid-Pliocene nannofossil assemblages. *Marine Micropaleontology*, 51(1-2): 39-56.

Giunta S., Morigi C., Negri A. & Guichard F. (2007) - Holocene biostratigraphy and paleoenvironmental changes in the Black Sea based on calcareous nannoplankton. *Marine Micropaleontology*, 63(1-2): 91-110.

Gradstein F.M., Ogg J.G., Schmitz M.D. & Ogg G.M. (2012) - The geologic time scale 2012. Elsevier.

Gradstein F.M., Ogg J.G., Schmitz M.D. & Ogg G.M. (2020) - Geologic time scale 2020. Elsevier.

Hilgen F.J. & Krijgsman W. (1999) - Cyclostratigraphy and astrochronology of the Tripoli diatomite formation (pre-evaporite Messinian, Sicily, Italy). *Terra Nova*, 11(1): 16-22.

Hilgen F.J. (1991) - Extension of the astronomically calibrated (polarity) time scale to the Miocene/Pliocene boundary. *Earth and Planetary Science Letters*, 107(2): 349-368.

Hilgen F.J. & Langereis C.G. (1988) - The age of the Miocene–Pliocene boundary at the Capo Rossello area (Sicily). *Earth and Planetary Science Letters*, 91: 214-222.

Hsü K.J., Cita M.B. & Ryan W.B.F. (1973) - The origin of Mediterranean evaporites. Initial Reports of the Deep-Sea Drilling Project, 13(2): 1203-1231.

Iaccarino S. & Papani G. (1979) - Il Messiniano dell'Appennino Settentrionale dalla Val d'Arda alla Val Secchia: stratigrafia e rapporti con il substrato e il Pliocene. Istituti di Geologia, Paleontologia, Geografia, Petrografia e Giacimenti Minerari, Mineralogia (Ed), Volume dedicato a Sergio Venzo. Università degli Studi di Parma, Parma: 15-46.

Iaccarino S., Castradori D., Cita M.B., Di Stefano E., Gaboardi S., McKenzie J.A., Spezzaferri S. & Sprovieri R. (1999) - The Miocene/Pliocene boundary and the significance of the earliest Pliocene flooding in the Mediterranean. *Memorie della Società Geologica Italiana*, 54(10): 109-131.

Imai R., Farida M., Sato T. & Iryu Y. (2015) - Evidence for eutrophication in the northwestern Pacific and eastern Indian oceans during the Miocene to Pleistocene based on the nannofossil accumulation rate, *Discoaster* abundance, and coccolith size distribution of *Reticulofenestra*. *Marine Micropaleontology*, 116: 15-27.

Kouwenhoven T.J., Morigi C., Negri A., Giunta S., Krijgsman W. & Rouchy J.M. (2006) - Paleoenvironmental evolution of the eastern Mediterranean during the Messinian: Constraints from integrated microfossil data of the Pissouri Basin (Cyprus). *Marine Micropaleontology*, 60(1): 17-44.

Laskar J., Robutel P., Joutel F., Gastineau M., Correia A. & Levrard B. (2004) - A long-term numerical solution for the insolation quantities of the Earth. *Astronomy and Astrophysics*, 428: 261-285.

Lirer F., Foresi L.M., Iaccarino S.M., Salvatorini G., Turco E., Cosentino C., Sierro F.J. & Caruso A. (2019) - Mediterranean Neogene planktonic foraminifer biozonation and biochronology. *Earth-Science Reviews*, 196: 102869.

Loget N., Driessche J.V.D. & Davy P. (2005) - How did the Messinian salinity crisis end? *Terra Nova*, 17(5): 414-419.

Lourens L.J., Antonarakou A., Hilgen F.J., Van Hoof A.A.M., Vergnaud-Grazzini C. & Zachariasse W.J. (1996) - Evaluation of the Plio-Pleistocene astronomical timescale. *Paleoceanography*, 11(4): 391-413.

Lozar F., Violanti D., Bernardi E., Dela Pierre F. & Natalicchio M. (2018) - Identifying the onset of the Messinian salinity crisis: a reassessment of the biochronostratigraphic tools (Piedmont Basin, NW Italy). *Newsletters on Stratigraphy*, 51(1): 11-31.

Lozar F., Violanti D., Dela Pierre F., Bernardi E., Cavagna S., Clari P., Irace A., Martinetto E. & Trenkwalder S. (2010) - Calcareous nannofossils and foraminifers herald the Messinian salinity crisis: the Pollenzo section (Alba, Cuneo; NW Italy). *Geobios*, 43(1): 21-32.

Mancini A.M., Gennari R., Ziveri P., Mortyn P.G., Stolwijk D.J. & Lozar F. (2020) - Calcareous nannofossil and foraminiferal trace element records in the Sorbas Basin: A new piece of the Messinian Salinity Crisis onset puzzle. *Palaeogeography, Palaeoclimatology, Palaeoecology*, 554: 109796.

Mancini A.M., Grelaud M., Ziveri P., Nallino E. & Lozar F. (2021) - Calcareous nannofossil size and abundance response to the Messinian Salinity Crisis onset and paleoenvironmental dynamics. *Paleoceanography and Paleoclimatology*, 36(9): e2020PA004155.

Mancini A., Nallino E. & Pilade F. (2023) - Toward a discrimination between reworked and in situ microfossil during the last phase of the Messinian Salinity Crisis: taphonomic insights from Maccarone Section (Central Italy). *Rendiconti Online della Società Geologica Italiana*, p. 60.

Mancini A. M., Myers S., Gennari R., Lozar, F. & Negri A. (2024) - The Messinian paleoenvironment in the Mediterranean (Monte dei Corvi, Ancona): a comparison with the modern oceanographic conditions. *Palaeogeography, Palaeoclimatology, Palaeoecology*, 112332.

Marzocchi A., Flecker R., Van Baak C.G., Lunt D.J. & Krijgsman W. (2016) - Mediterranean outflow pump: An alternative mechanism for the Lago-mare & the end of the Messinian Salinity Crisis. *Geology*, 44(7): 523-526.

Mosca P., Polino R., Rogledi S. & Rossi M. (2010) - New data for the kinematic interpretation of the Alps-Apennines junction (Northwestern Italy). *International Journal of Earth Sciences*, 99(4): 833-849.

Perch-Nielsen K. (1985) - Cenozoic calcareous nannofossils. In: Bolli H.M., Saunders J.B. & Perch-Nielsen K. (Eds.) - Plankton stratigraphy: planktic foraminifera, calcareous nannofossils and calpionellids (Vol. 1). Cambridge Earth Science Series: 427-455.

Pérez-Asensio J.N., Aguirre J., Jiménez-Moreno G., Schmiedl G. & Civis J. (2013) - Glacioeustatic control on the origin and cessation of the Messinian salinity crisis. *Global and Planetary Change*, 111: 1-8.

Pierre C., Caruso A., Blanc-Valleron M.M., Rouchy J.M. & Orzsag-Sperber F. (2006) - Reconstruction of the paleoenvironmental changes around the Miocene-Pliocene boundary along a West-East transect across the Mediterranean. *Sedimentary Geology*, 188: 319-340.

Pilade F., Vasiliev I., Birgel D., Dela Pierre F., Natalicchio M., Mancini A., Carnevale G. & Gennari R. (2023) - Deciphering the termination of the Messinian salinity crisis: The alkenone record of the Miocene-Pliocene transition in the northern Mediterranean. *Palaeogeography, Palaeoclimatology, Palaeoecology*, 631: 111831.

Popov S.V., Bugrova E.M., Amitrov O.V., Andreyeva-Grigorovich A.S., Akhmetiev M.A., Zaporozhets N.I., Nikolaeva I.A., Sychevskaja E.K. & Shcherba I.G. (2004) - Biogeography of the northern peri-tethys from the late Eocene to the early Miocene. Part 3. Late oligocene-early miocene. Marine basins. *Paleontological journal*, 38: Suppl. 6, 2004: S653-S7J6.

Raffi I., Wade B.S., Pälike H., Beu A.G., Cooper R., Crundwell M.P., Krijgsman W., Moore T., Raine I., Sardella R. & Vernyhorova Y.V. (2020) - The neogene period. In Geologic time scale 2020: 1141-1215. Elsevier.

Rio D., Raffi I. & Villa G. (1990) - Pliocene-Pleistocene Calcareous Nannofossil distribution patterns in the Western Mediterranean. In: Kasten K., Mascle J. et al. - Proceedings of the Ocean Drilling Program, Scientific Results, 107: 513-533. College Station TX: Ocean Drilling Program.

Rossi M., Mosca P., Polino R., Rogledi S. & Biffi U. (2009) - New outcrop and subsurface data in the Tertiary Piedmont Basin (NW-Italy): unconformity-bounded stratigraphic units and their relationships with basin-modification phases. *Rivista Italiana di Paleontologia e Stratigrafia*, 115(3): 305-335.

Rouchy J.M., Orszag-Sperber F., Blanc-Valleron M.M., Pierre C., Rivière M., Combourieu-Nebout N. & Panayides I. (2001) - Paleoenvironmental changes at the Messinian–Pliocene boundary in the eastern Mediterranean (southern Cyprus basins): significance of the Messinian Lago-Mare. *Sedimentary Geology*, 145(1-2): 93-117.

Roveri M., Flecker R., Krijgsman W., Lofi J., Lugli S., Manzi V., Sierro F.J., Bertini A., Camerlenghi A., De Lange G., Govers R., Hilgen F.J., Hübscher C., Meijer P. & Stoica M. (2014) - The Messinian Salinity Crisis: past and future of a great challenge for marine sciences. *Marine Geology*, 352: 25-58.

Roveri M. & Manzi V. (2006) - The Messinian salinity crisis: looking for a new paradigm? *Palaeogeography, Palaeoclimatology, Palaeoecology*, 238(1-4): 386-398.

Roveri M., Gennari R., Persico D., Rossi F.P., Lugli S., Manzi V., Reghizzi M. & Taviani M. (2019) - A new chronostratigraphic and palaeoenvironmental framework for the end of the Messinian salinity crisis in the Sorbas Basin (Betic Cordillera, southern Spain). *Geological Journal*, 54(3): 1617-1637.

Ryan W.B. (2023) - 50th anniversary review of the Mediterranean desiccation hypothesis. *La Rivista del Nuovo Cimento*, 1-129.

Sabino M., Birgel D., Natalicchio M., Dela Pierre F. & Peckmann J. (2022) - Carbon isotope excursions during the late Miocene recorded by lipids of marine Thaumarchaeota, Piedmont Basin, Mediterranean Sea. *Geology*, 50(1): 32-36.

Schiebel R. & Hemleben C. (2017). Planktic foraminifers in the modern ocean (Vol. 358). Berlin: Springer.

Schueth J.D. & Bralower T.J. (2015) - The relationship between environmental change and the extinction of the nannoplankton *Discoaster* in the early Pleistocene. *Paleoceanography*, 30(7): 863-876.

Sierro F.J., Hilgen F.J., Krijgsman W. & Flores J.A. (2001) - The Abad composite (SE Spain): a Messinian reference section for the Mediterranean and the APTS. *Palaeogeography, Palaeoclimatology, Palaeoecology*, 168(1-2): 141-169.

Sierro F.J., Flores J.A., Francés G., Vazquez A., Utrilla R., Zamarreno I., Erlenkeuser H. & Barcena M.A. (2003) - Orbitally controlled oscillations in planktic communities and cyclic changes in western Mediterranean hydrography during the Messinian. *Palaeogeography, Palaeoclimatology, Palaeoecology*, 190: 289-316.

Spezzaferri S., Coxall H.K., Olsson R.K. & Hemleben C. (2018) - Taxonomy, biostratigraphy, and phylogeny of Oligocene *Globigerina*, *Globigerinella*, and *Quiltyella* n. gen. Cushman Foundation Special Publication, 46: 179-214.

Srinivasan M.S. & Kennett J.P. (1983) - The Oligocene-Miocene boundary in the South Pacific. *Geological Society of America Bulletin*, 94(6): 798-812.

Sturani C. (1978) - Messinian facies in the Piedmont Basin. *Memorie della Società Geologica Italiana*, 16: 11-25.

Takahashi K. & Okada H. (2000) - Environmental control on the biogeography of modern coccolithophores in the southeastern Indian Ocean offshore of Western Australia. *Marine Micropaleontology*, 39(1-4): 73-86.

Trenkwalder S., Violanti D., D'Atri A., Lozar F., Dela Pierre F. & Irace A. (2008) - The Miocene/Pliocene boundary and the early Pliocene micropalaeontological record: new data from the Tertiary Piedmont Basin (Moncucco quarry, Torino Hill, Northwestern Italy). *Bollettino della Società Paleontologica Italiana*, 47, 2.

Van Couvering J. A., Castradori D., Cita M. B., Hilgen F. J. & Rio D. (2000) - The base of the Zanclean Stage and of the Pliocene Series. *Episodes Journal of International Geoscience*, 23(3): 179-187.

Van der Laan E., Snel E., De Kaenel E., Hilgen F. J. & Krijgsman W. (2006) - No major deglaciation across the Miocene-Pliocene boundary: integrated stratigraphy and astronomical tuning of the Loulja sections (Bou Regreg area, NW Morocco). *Paleoceanography*, 21, PA3011, doi:10.1029/2005PA001193.

Van Dijk G., Maars J., Andreetto F., Hernández-Molina F. J., Rodríguez-Tovar F. J. & Krijgsman W. (2023) - A terminal Messinian flooding of the Mediterranean evidenced by contouritic deposits on Sicily. *Sedimentology*, 70: 1195-1223, doi: 10.1111/sed.13074

Violanti D., Dela Pierre F., Trenkwalder S., Lozar F., Clari P., Irace A. & D'Atri A. (2011) - Biostratigraphic and palaeoenvironmental analyses of the Messinian/Zanclean boundary and Zanclean succession in the Moncucco quarry (Piedmont, northwestern Italy). *Bulletin de la Société géologique de France*, 182(2): 149-162.

Violanti D., Trenkwalder S., Lozar F. & Gallo L. M. (2009) - Micropalaeontological analyses of the Narzole core: biostratigraphy and palaeoenvironment of the late Messinian and early Zanclean of Piedmont (Northwestern Italy). *Bollettino della Società Paleontologica Italiana*, 48(3):

167-181.

Wade B. S. & Bown P. R. (2006) - Calcareous nannofossils in extreme environments: the Messinian salinity crisis, Polemi Basin, Cyprus. *Palaeogeography, Palaeoclimatology, Palaeoecology*, 233(3-4): 271-286.

Young J. R. (1998) - Neogene nannofossils. In: Brown P. (Ed.) - Calcareous Nannofossil Biostratigraphy. British Micropaleontology Society Publications Series, Cambridge: Kluwer Academic Publisher: 225-265.

Young J.R., Bown P.R. & Lees J.A. (2022) - Nannotax3 website. International Nannoplankton Association. Last accessed 21 Apr. 2022.

Ziveri P., Baumann K. H., Böckel B., Bollmann J. & Young J. R. (2004) - Biogeography of selected Holocene coccoliths in the Atlantic Ocean. In: Thierstein H. & Young J. (Eds.) - Coccolithophores: from molecular processes to global impact: 403-428. Springer Verlag.